

Non-contact surface thermal deformation measurement based on chromatic confocal sensor

XIAOXIAO MAO, ZHIMING XING, BIN ZHAO, FEI SUN, XIUMIN GAO*

University of Shanghai for Science and Technology, Shanghai 200093, China

*Corresponding author: gxm@usst.edu.cn

Chromatic confocal sensors are widely used in chip processing, high-precision instrument manufacturing, industrial testing and other fields because of high-precision displacement recognition capabilities. This research combines a chromatic confocal device with resistance temperature detector for dynamic deformation measurement of heating pipeline. The system is suitable for the measuring range of 300 μm and resolution can reach 0.3 μm . Using finite element method to simulate thermal deformation of aluminium with a thickness of 2 mm, and obtaining simulation trends and results. The end face of aluminium is heated continuously and uniformly in experiment, recording the data of spectral, laser triangular displacement sensor, and temperature sensor at 10°C intervals, respectively. And using Gaussian fitting algorithm to obtain spectral peaks, the corresponding thermal deformation is obtained through the relationship between wavelength and axial displacement. The results show that the experimental data of the chromatic confocal sensor is consistent with the laser triangular displacement sensor basically, with a maximum standard deviation of 1.06. In addition, simulation and experimental trends are consistent.

Keywords: chromatic confocal sensor, laser triangular displacement sensor, thermal deformation measurement, finite element method.

1. Introduction

Pipelines have been applied in various fields and are important transportation tools for oil, natural gas, and various petroleum products with the development of production technology [1]. However, long-term use and the complex environmental conditions have a significant impact on its deformation [2]. In case the malfunctions occur, they may still lead to productions losses, fires, casualties, and ecological pollution. The “thermal expansion” caused by temperature is one of the most inevitable causes of pipelines deformation [3], and it is also urgent to be solved in the measurement of pipelines surface deformation.

The thermal deformation of pipelines can be evaluated by measuring the strain. While the traditional installation method of electric strain gauges is complex and greatly affected by factors such as electromagnetic and temperature [4], which cannot meet the requirements of pipelines deformation measurement at high temperatures, currently. In recent years, many scientists have proposed methods based on finite el-

ement method (FEM) to calculate the stress and deformation of pipelines under different temperature loads and boundary conditions [5-7]. They used FEM to study the deformation of pipelines, which have significance for practical measurements. In addition, measurement methods of non-contact optical deformation are also widely used, such as optical coherence tomography [8], laser interferometry [9], electronic speckle pattern method [10], laser displacement method [11], grating interferometry [12], *etc.* However, the above methods have strict requirements for optical systems, environment and there are defects such as operational hazards. In response to the above issues, a non-contact surface thermal deformation measurement based on chromatic confocal sensor (CCS) is proposed.

CCS establishes the correspondence between distance and wavelength through the principle of optical dispersion, which is one of the most promising methods in displacement measurement [13]. It has been widely used in thickness, morphology, displacement and other detection fields [14-18]. COX *et al.* proposed the method of confocal thickness to measure thin transparent coatings on optical disks [19]. ZHOU *et al.* used CCS to measure the thickness of a flat-water falling film, which indicated a good agreement with theoretical results [20]. ZSCHENDERLEIN *et al.* measured the elastic expansion deformation of thin films under dynamic pressure in the high-temperature range of 150°C with chromatic confocal technology (CCT) [21]. LIU *et al.* constructed an accurate contour and thickness measurement device based on CCT [22], while TANG *et al.* developed a target inner surface contour measurement system based on CCT, achieving precise measurement of surface contour in the target inner [23]. Obviously, the application range of CCS is gradually expanding due to unique axial response and high-precision displacement recognition ability. However, using CCS to measure pipeline thermal deformation and analyse temperature changes have rarely been researched.

In this paper, we propose a CCS combined with platinum resistance temperature detector (Pt RTD) to measure surface deformation in a heating environment, by introducing a thermal deformation temperature model and simulating the thermal deformation process to be analysed comprehensively. The measurement results of CCS are compared with laser triangular displacement sensor (LTDS), and we discuss the feasibility of the experimental method.

2. Theoretical analysis

2.1. Principle of chromatic confocal measurement

Schematic diagram of chromatic confocal system is shown in Fig. 1. The light emitted from the light source is modulated into a point source by the illumination pinhole. Due to the dispersion effect of the dispersion objective, the polychromatic light entering the system will focus at different axial positions after passing through the dispersion objective. When the light is reflected from the original path of the object surface, only the part focused on the focal plane can pass through the detection pinhole to enter the detector, other light is blocked by the pinhole. The confocal method mainly according to the wavelength of the light focused on the surface of the object changes with the

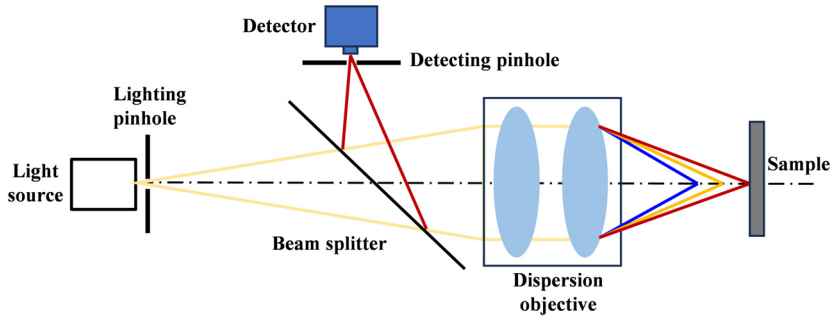


Fig. 1. Schematic diagram of chromatic confocal system.

displacement of the surface, and the detector receives the reflected light focused on the focal plane. Here, the focal points of the light source, detector and object space are conjugated.

The linear relationship between wavelength λ_i and its focal position $f(\lambda_i)$ is [24]:

$$f(\lambda_i) = k\lambda_i + z \tag{1}$$

According to the dispersion characteristics, the light intensity at the confocal pinhole can be represented by the following equation [25]:

$$I(u) = \left[\frac{\sin(u/4)}{u/4} \right]^4 \tag{2}$$

Where u can also be defined as:

$$u = \frac{2\pi}{\lambda(z)} \Delta z \frac{a^2}{f^2} \tag{3}$$

In Eq. (3), u is the normalized axial optical coordinate, a is the aperture of the imaging lens, λ is the wavelength of the incident light, f is the focal length of the imaging lens, and Δz is the axial defocus. Thus, the axial displacement of the object can be obtained by collecting the peak value of the reflected light on the surface of the object and establishing a linear relationship according to Eq. (1). When the axial displacement of an object is Δl , it can be expressed as:

$$\Delta l = f(\lambda_2) - f(\lambda_1) \tag{4}$$

In this case, λ_1 is the focus wavelength of the initial position, λ_2 is the focal wavelength after the displacement of the object.

2.2. Theoretical analysis of thermal deformation

When an object undergoes thermal deformation, the internal structure will expand or contract accordingly, resulting in stress generation due to mutual constraints among

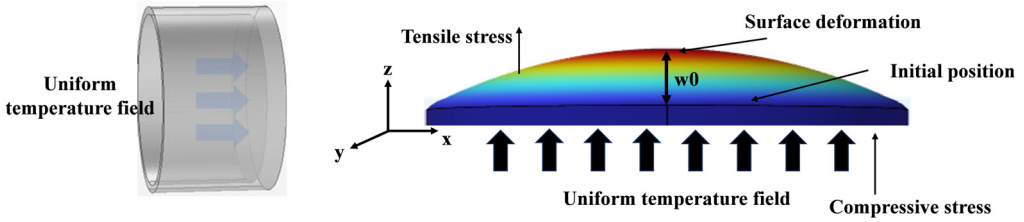


Fig. 2. Schematic diagram of thermal deformation.

internal components. The experiment adopts an aluminium pipeline with dimensions of 98 mm × 55 mm and thickness of 2 mm, which is fixed radially. Uniform temperature field heats the end face of the pipeline as illustrated in Fig. 2.

Assuming that the selected aluminium pipeline is uniform, continuous, and isotropic, with the same material elastic modulus, which satisfies Hooke's law that strain and stress are proportional [26]. The end face of the pipeline can be seen as an axisymmetric object according to the actual medium parameters. Any plane passing through this axis is symmetrical, regardless of shape, constraints, or external forces. So, all stresses, strains, and displacements are symmetrical about that axis. This is axisymmetric problem, and the equilibrium equation of a spatially axisymmetric object can be expressed as [27]:

$$\begin{cases} \frac{\partial \sigma_r}{\partial r} + \frac{\partial \tau_{zr}}{\partial z} + \frac{\sigma_r - \sigma_\theta}{r} = 0 \\ \frac{\partial \sigma_z}{\partial z} + \frac{\partial \tau_{zr}}{\partial r} + \frac{\tau_{zr}}{r} = 0 \end{cases} \quad (5)$$

Due to the external constraints and internal mutual constraints, the free deformation cannot occur in the object. For uniformly isotropic objects, temperature only causes positive strain and does not produce shear strain under free expansion or contraction conditions. Therefore, the formula can also be transformed into a function of strain and temperature difference to represent stress [28]:

$$\begin{cases} \sigma_r = 2G \left[\frac{1-\mu}{1-2\mu} \frac{\partial u}{\partial r} + \frac{\mu}{1-2\mu} \left(\frac{u}{r} + \frac{\partial w}{\partial z} \right) \right] - \beta T \\ \sigma_\theta = 2G \left[\frac{1-\mu}{1-2\mu} \frac{u}{r} + \frac{\mu}{1-2\mu} \left(\frac{\partial w}{\partial z} + \frac{\partial u}{\partial r} \right) \right] - \beta T \\ \sigma_z = 2G \left[\frac{1-\mu}{1-2\mu} \frac{\partial w}{\partial z} + \frac{\mu}{1-2\mu} \left(\frac{\partial u}{\partial r} + \frac{u}{r} \right) \right] - \beta T \\ \tau_{zr} = G \left(\frac{\partial w}{\partial r} + \frac{\partial u}{\partial z} \right) \end{cases} \quad (6)$$

where:

$$G = \frac{E}{2(1 + \mu)}$$

$$\beta = \frac{E\alpha}{1 - 2\mu}.$$

Due to the small aspect ratio of the end face of pipeline in the experiment, it can be approximated as a plane problem in elasticity. The temperature field uniformly heats the end face of the pipeline, where w, u are only a function of r and the temperature T is a function of r, z . Therefore, we can obtain:

$$T = T(r, z) \quad (7)$$

By substituting the expression given by Eqs. (6)–(7) into Eq. (5), it can be concluded that:

$$-\beta \frac{\partial T}{\partial z} + G \frac{\partial^2 w}{\partial r^2} + \frac{G}{r} \frac{\partial w}{\partial r} = 0 \quad (8)$$

It is evident that the axial deformation of the pipeline end face caused by the temperature change can be determined, if the distribution function of temperature is known. However, it is generally not easy to solve in reality. There are various disturbances, we must use the stress function and thermoelastic displacement potential to address this issue.

3. Methods

3.1. Finite element numerical simulation

FEM was used to simulate the aluminium tube based on the thermal deformation theory analysis introduced in the second section. A pipeline model with the same size as the real one was created, the thickness of surface to be measured is 2 mm and the other side was connected to air, as shown in Fig. 3 (a). The default is that the thermal ex-

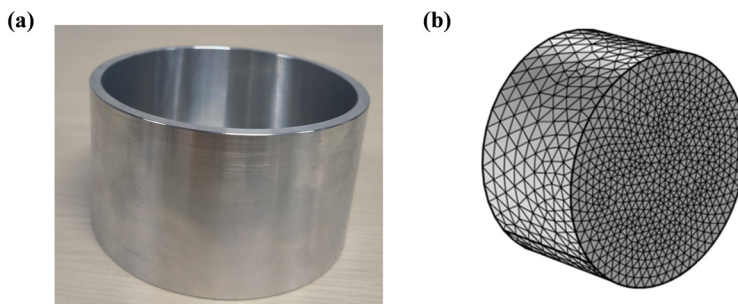


Fig. 3. Pipeline diagram. (a) Real pipeline diagram, and (b) surface mesh division diagram.

T a b l e 1. Thermal and physical parameters of aluminium pipeline.

	Density	Elastic modulus	Poisson's ratio	Thermal expansion coefficient
Aluminium	2700 kg/m ³	7.0 × 10 ¹⁰ Pa	0.33	2.3 × 10 ⁻⁵ K

pansion coefficient of aluminium is constant under low temperature simulation at around 120°C. In order to simplify the model and improve the computational efficiency of FEM, the mesh division of the pipeline structure is shown in Fig. 3 (b).

The sides of aluminium pipeline were fixed and placed in a static environment. A heat source diameter of 90 mm was applied on the inner surface of the end face, which heated the pipeline continuously. According to Eq. (8), the axial thermal deformation of the end face was related to the position of the measurement point. Figure 4 shows the curves of temperature and centered displacement of aluminium pipeline end face during the heating process of uniform temperature field calculated by using FEM. From the fitting results, the axial displacement increases linearly with the temperature of the aluminium tube end face, which is consistent with the theory of thermal deformation.

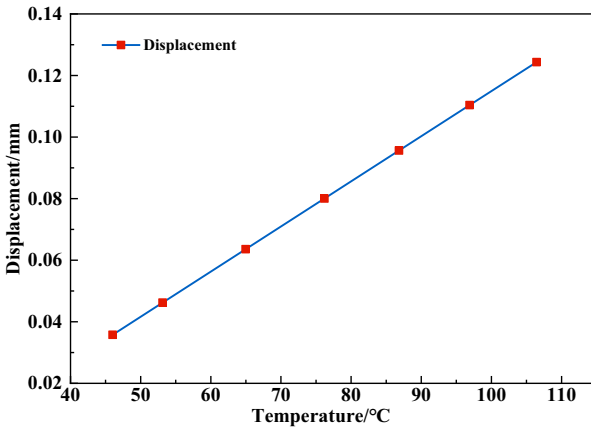
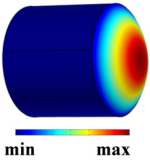


Fig. 4. Curve of central axial displacement and temperature.

T a b l e 2. Simulation results of aluminium pipeline.

	Temperature [°C]	Displacement [mm]
	46	0.0357
	53	0.0462
	65	0.0635
	75	0.0800
	86	0.0956
	95	0.1104
	106	0.1243

The experimental rules are easy to grasp due to the relatively large expansion coefficient of aluminium, thus the stress state of the calculation model heated to around 120°C is sufficient. The simulated results of the deformation of the aluminium pipeline end face are shown in Table 2, and the colour of the ring represents the size of the displacement. According to Table 2, the axial displacement of the aluminium tube end face shows a phenomenon of large centre displacement, small edge displacement, and radial variation. Therefore, we can ignore the small displacement of the edge and focus on measuring the central position to predict deformation in the actual study.

3.2. Experiment and analysis

3.2.1. Experimental device

The thermal expansion experiment of the aluminium pipeline was carried out in the device shown in Fig. 5, which was established on a stable optical platform. The first part of the system is for heating and controlling the temperature of the aluminium pipeline, the second part is the chromatic confocal system, which is the core of the whole system to measure the thermal deformation of the end face. The third part is the LTDS, which is helpful to verify the feasibility of the chromatic confocal system method by comparing the results measured in the second part. The experimental optical source system utilizes Thorlabs' MWWHF2 fiber-coupled light source, Y-shaped optical fiber with a numerical aperture of 0.22 used as illumination pinhole to filter the white light source and the port in front of the spectrometer serves as the detection pinhole to shield

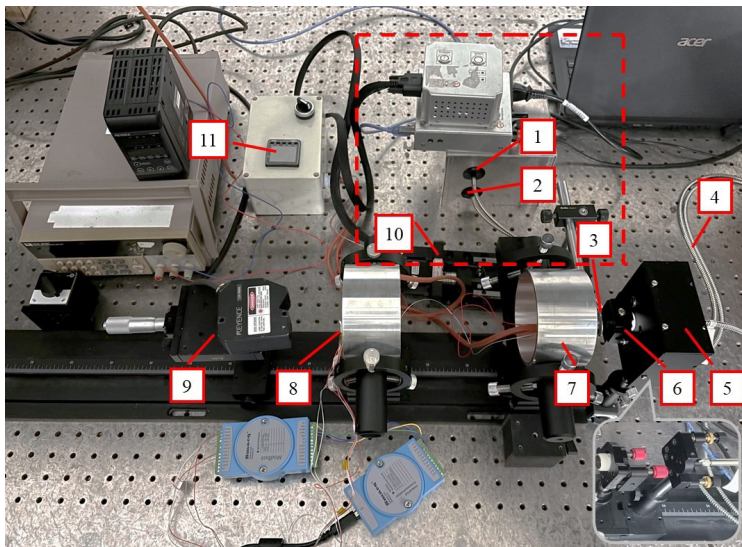


Fig. 5. Experimental device to measure the deformation. (1) Light source, (2) spectrometer, (3) calibration gasket, (4) Y-shaped optical fiber, (5) collimating lens, (6) dispersive lenses, (7) aluminium pipeline, (8) platinum resistance temperature detector, (9) laser triangulation displacement sensor, (10) motorized stage, and (11) temperature controller.

the defocused light. The collimating lens of SMA905 interface is used to collimate the light.

During the experiment, heating elements were pasted on the end face of the aluminium pipeline, and the two aluminium pipelines were heated at the same time. The thermal deformation is measured on one side by LTDS (LK-H050 Keyence), with a repeatability of $0.025\ \mu\text{m}$, an accuracy of $2\text{--}3\ \mu\text{m}$, and a measurement range of $\pm 10\ \text{mm}$. Meanwhile, the other side was measured by self-developed chromatic confocal system. The visible band of objective is $450\text{--}650\ \text{nm}$, with a focal distance of $25\ \text{mm}$, and a linear range of $0.3\ \text{mm}$. The external surface temperature of the pipelines can be obtained with Pt RTD, which were attached to the centre and the edge of the pipeline end face, respectively.

3.2.2. Calibration experiments

Due to the processing error of dispersive objective lens, mechanical assembly and other problems, the actual experiment and the theoretical results are different. Therefore, it is necessary to obtain an accurate calibration curve for measuring the end face deformation of pipeline. A standard stainless-steel gasket with high reflectivity is placed on the electronic control translation platform (GCD-402050M), as shown by the red wireframe in Fig. 5. Firstly, the gasket was placed in a suitable position, and the stepper motor drove at intervals of $50\ \mu\text{m}$, with a step accuracy of $2.5\ \mu\text{m}$. Then a spectrometer was used to record the spectral signals at different positions. The repeatability of the motorized translation stage is $1\ \mu\text{m}$ in the measuring range of $50\ \text{mm}$, and both the measuring range and motion accuracy meet the experimental requirements.

In order to reduce errors at each CCS position, spectral data were acquired 10 times and averaged. The peak wavelengths were extracted based on Gaussian fitting algorithm, and the wavelength and axial displacement data are linearly fitted in Fig. 6.

Based on the calibration module, we further studied the resolution of the system using the gasket as the measured object. Considering the experimental instrument pa-

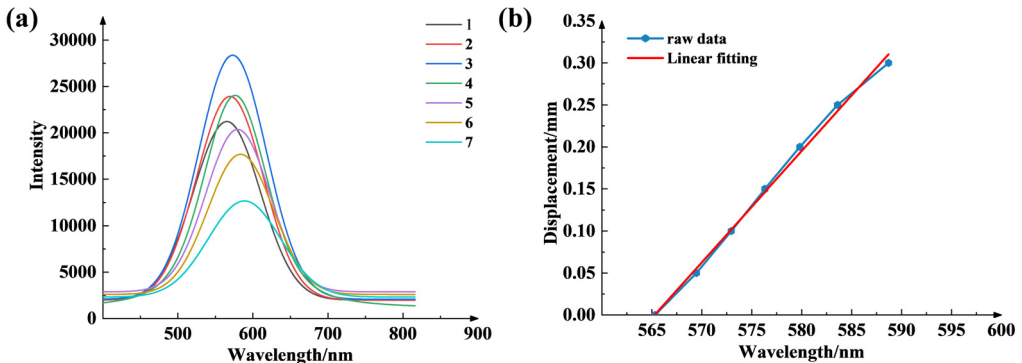


Fig. 6. Results of the calibration experiments. (a) Different axial positions correspond to spectra, and (b) the least squares fitting results.

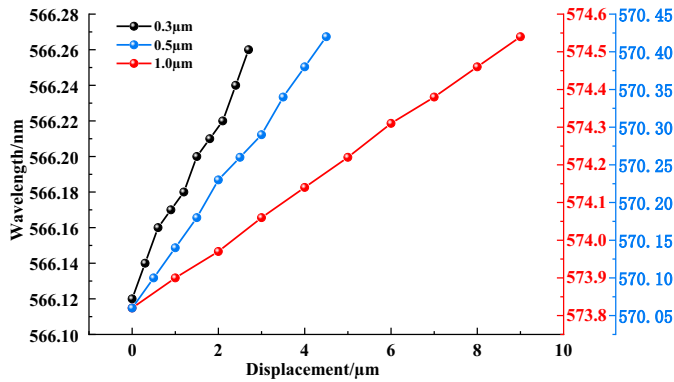


Fig. 7. Experimental results of system resolution.

rameters, the translation stage was driven along the axis at intervals of 1, 0.5 and 0.3 μm , respectively, and the spectral peak value is extracted based on Gaussian fitting, as illustrated in Fig. 7.

From Fig. 7, the system can remain stable at 1.0 μm . When the step size is shortened to 0.5 μm it still remains stable, but when the step size is 0.3 μm , the curve begins to appear as a stepped shape. Thus, the resolution in this experiment is at least 0.3 μm .

3.2.3. Experimental results and analysis of thermal deformation

The experiment was located in an optical darkroom, and the right pipeline was slowly moved to the focus range. After completing the above steps, we collected the spectral signal at this position as the initial value. The heating elements have a very high heating power after being connected to the power supply, which results that the temperature is not uniform. After powering off, the temperature decreases slowly relatively, which can be considered as the temperature of the heating element being uniform. Therefore, the experiment collected the deformation during the cooling process. The heating device stopped heating when position 1 of Pt RTD detected that the temperature at the end face of the pipeline increased to around 120°C, and when it dropped to about 110°C, corresponding spectral data of CCS and LTDS was collected with a collection interval of 10°C.

Typically, we used displacement to depict changes in position. Heating causes the centre of the pipeline end face to bulge, and as the temperature decreases, the pipeline returns to its original state, and the degree of deformation gradually decreases. The temperature curves collected by the thermocouples in the heating-cooling process are shown in Fig. 8(a). It can be seen that the temperature at the centre position of the pipeline is higher than that at the edge position. There are two peaks in Fig. 8(b), one of which is the peak of the light source, and will not be studied in the experiment. The end face deformation caused by temperature causes the displacement of the second peak

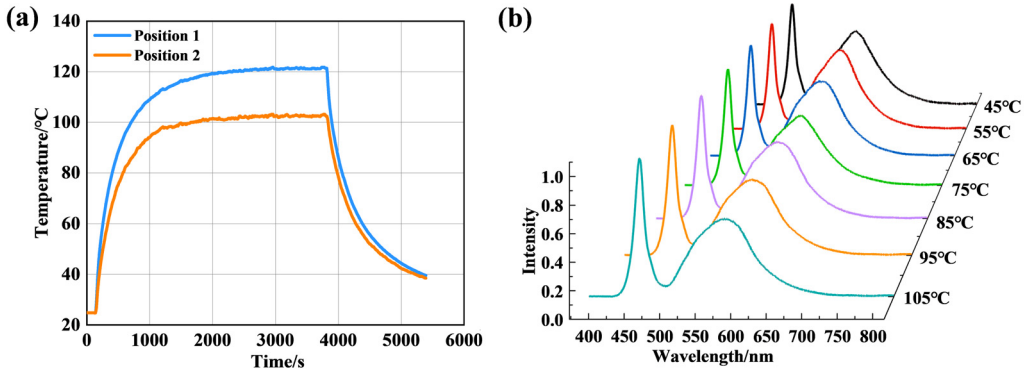


Fig. 8. Results of thermal deformation experiment. (a) Temperature curve collected by thermocouple, and (b) spectrograms corresponding to deformation of 45 to 105°C.

position of the spectrum, and the axial displacement corresponding to the peak wavelength of the spectrum is the deformation value.

The peak value of the measured spectrum was extracted by Gaussian fitting, and substituted into Eq. (9) to calculate the deformation of each temperature. The comparison of measurement results between CCS and LTDS is presented in Table 3.

T a b l e 3. Comparison of LTDS with results from the CCS.

Temperature [°C]	45	55	65	75	85	95	105
LTDS [μm]	33	45	58	72	87	96	110
CCS [μm]	31.13	43.05	56.18	74.15	84.80	98.45	107.59
Difference [μm]	-1.87	-1.95	-1.82	2.15	-2.20	2.45	-2.41

It can be observed from the table that the deformation values of the CCS are essentially consistent with the LTDS, which proves the reliability of the CCS for thermal deformation measurement. In addition, the axial displacement of the centre point obtained by the experiments within the range of FEM results, and has the same magnitude. Due to the transient nature of the simulation, the temperature cannot be completely consistent with the experiment.

In order to demonstrate the reliability and precision of the experimental results, the pipeline is tested several times, with each measurement interval long enough to ensure that the experimental device is cooled to room temperature. The measurement errors for the four instances of CCS and LTDS are depicted in Fig. 9(a), while Fig. 9(b) illustrates the standard deviations.

From Fig. 9, it can be observed that as the temperature increases, the measured error in the results also increases. The maximum standard deviation is 1.06. That is because with the increase of surface deformation and curvature of the object, the larger the drift of the spot on the image surface occurs.

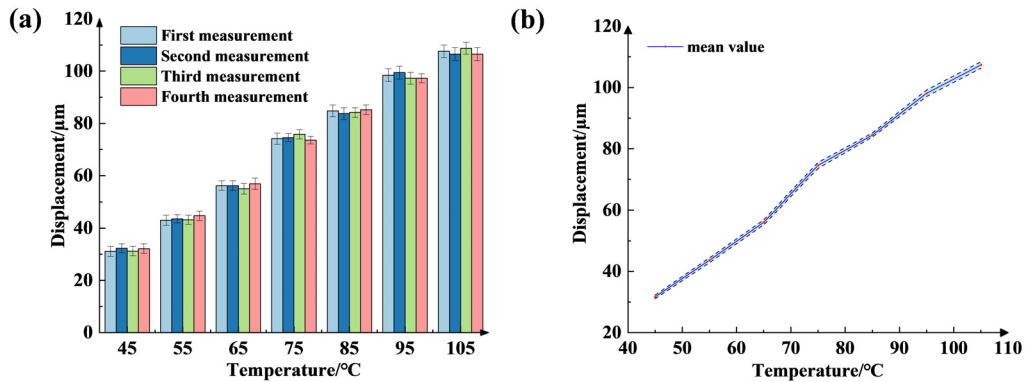


Fig. 9. Four repeated experimental measurement results. (a) Measurement error of CCS and LTDS, and (b) Variance in the CCS measurements.

4. Conclusions

In summary, this paper investigated a non-contact surface thermal deformation measurement based on CCS. The self-developed dispersive objective is combined with Pt RTD and LTDS to construct a system for measuring surface deformation in a heating environment.

The central axial deformation value between 45 and 105°C was obtained by analysing the axial response curves measured by the spectrometer. Comparing the data of CCS from the LTDS, the maximum error is 2.45 μm, and it was within the range of the simulation data. Therefore, the chromatic confocal method is a feasible and effective method for measuring surface thermal deformation, which can be widely applied in high-precision detection of mechanical parts, electronic components, and other fields.

Acknowledgements

This work was supported by the National Key Research and Development Program of China (2018YFC1313803).

Disclosures

The authors declare no conflicts of interest.

Data availability

Data underlying the results presented in this paper are not publicly available at this time but may be obtained from the authors upon reasonable request.

References

- [1] VISHNUVARDHAN S., MURTHY A.R., CHOUDHARY A., *A review on pipeline failures, defects in pipelines and their assessment and fatigue life prediction methods*, International Journal of Pressure Vessels and Piping **201**, 2023: 104853. <https://doi.org/10.1016/j.ijpvp.2022.104853>

- [2] MAHJOUBI S., TAN X., BAO Y., *Inverse analysis of strain distributions sensed by distributed fiber optic sensors subject to strain transfer*, Mechanical Systems and Signal Processing **166**, 2022: 108474. <https://doi.org/10.1016/j.ymssp.2021.108474>
- [3] ZHU X.M., FENG S.K., HUANG T., SHANG F., YANG L.F., *Deformation inspection and safety assessment method of buried flexible pipeline in service*, IOP Conference Series: Materials Science and Engineering **1043**(4), 2021: 042043. <https://doi.org/10.1088/1757-899X/1043/4/042043>
- [4] LI G.H., MA W.L., ZHU T.T., FU Z., GE P.X., *Thermal deformation measurement of hollow disk based on digital image correlation method*, Laser & Optoelectronics Progress **58**(14), 2021: 1412003.
- [5] CHEN J.H., ZHANG G.M., QIU Q.Q., CHEN X.G., TENG, Y.P., JING L.W., SONG N.H., *Simulation and experiment on superconducting DC energy pipeline cooled by LNG*, Cryogenics **112**, 2020: 103128. <https://doi.org/10.1016/j.cryogenics.2020.103128>
- [6] ZHANG D., GUAN M.S., ZHANG Q.D., WANG A.G., ZHOU X.L., *Simulation study on steel pipe deformation behavior in retained mandrel pipe mill*, Journal of Physics: Conference Series **1633**(1), 2020: 012163. <https://doi.org/10.1088/1742-6596/1633/1/012163>
- [7] ZHAO B., LI J.Y., MAO X.X., SUN F., GAO X.M., *Dynamic pressure surface deformation measurement based on a chromatic confocal sensor*, Applied Optics **62**(6), 2023: 1467-1474. <https://doi.org/10.1364/AO.482808>
- [8] EDWARDS A.M.J., ATKINSON P.S., CHEUNG C.S., LIANG H., FAIRHURST D.J., OUALI F.F., *Density-driven flows in evaporating binary liquid droplet*, Physical Review Letters **121**(18), 2018: 184501. <https://doi.org/10.1103/PhysRevLett.121.184501>
- [9] JANG Y.S., WANG G., HYUN S., KANG H.J., CHUN B.J., KIM Y.J., KIM S.W., *Comb-referenced laser distance interferometer for industrial nanotechnology*, Scientific Reports **6**(1), 2016: 31770. <https://doi.org/10.1038/srep31770>
- [10] DONG C.Z., LI K., JIANG Y.X., AROLA D., ZHANG D.S., *Evaluation of thermal expansion coefficient of carbon fiber reinforced composites using electronic speckle interferometry*, Optics Express **26**(1), 2018: 531-543. <https://doi.org/10.1364/OE.26.000531>
- [11] WU C.X., CHEN B.J., YE C.S., YAN X.P., *Modeling the influence of oil film, position and orientation parameters on the accuracy of a laser triangulation probe*, Sensors **19**(8), 2019: 1844. <https://doi.org/10.3390/s19081844>
- [12] LIN J., GUAN J., WEN F., TAN J., *High-resolution and wide range displacement measurement based on planar grating*, Optics Communications **404**, 2017: 132-138. <https://doi.org/10.1016/j.optcom.2017.03.012>
- [13] CHMELIK R., LOVICAR L., HARNA Z., *Surface profilometry by a holographic confocal microscopy*, Optica Applicata **33**(2-3), 2003: 381-389.
- [14] ZHANG Y.L., YU Q., SHANG W.J., WANG C., LIU T., WANG Y., CHENG F., *Chromatic confocal measurement system and its experimental study based on inclined illumination*, Chinese Optics **15**(3), 2022: 514-524. <https://doi.org/10.37188/CO.2021-0181>
- [15] ZOU X.C., ZHAO X.S., LI G., LI, Z.Q., SUN T., *Non-contact on-machine measurement using a chromatic confocal probe for an ultra-precision turning machine*, The International Journal of Advanced Manufacturing Technology **90**, 2017: 2163-2172. <https://doi.org/10.1007/s00170-016-9494-3>
- [16] LI S.B., SONG B.F., PETERSON T., HSU J., LIANG R.G., *MicroLED chromatic confocal microscope*, Optics Letters **46**(11), 2021: 2722-2725. <https://doi.org/10.1364/OL.427477>
- [17] JURKO J., MIŠKIV-PAVLÍK M., HUSÁR J., MICHALIK P., *Turned surface monitoring using a confocal sensor and the tool wear process optimization*, Processes **10**(12), 2022: 2599. <https://doi.org/10.3390/pr10122599>
- [18] MA Y.D., XIAO Y.C., WANG Q.Q., YAO K., WANG X.R., ZHOU Y.P., LIU Y.C., SUN Y., DUAN, J., *Applications of chromatic confocal technology in precision geometric measurement of workpieces*, Journal of Physics: Conference Series **2460**, 2023: 012077. <https://doi.org/10.1088/1742-6596/2460/1/012077>
- [19] COX G., SHEPPARD C.J.R., *Measurement of thin coatings in the confocal microscope*, Micron **32**(7), 2001: 701-705. [https://doi.org/10.1016/S0968-4328\(01\)00017-8](https://doi.org/10.1016/S0968-4328(01)00017-8)

- [20] ZHOU D.W., GAMBARYAN-ROISMAN T., STEPHAN P., *Measurement of water falling film thickness to flat plate using confocal chromatic sensing technique*, *Experimental Thermal and Fluid Science* **33**(2), 2009: 273-283. <https://doi.org/10.1016/j.expthermflusci.2008.09.003>
- [21] ZSCHENDERLEIN U., ZHANG H., ECKE R., JÖHRMANN N., WUNDERLE B., *Dynamical characterisation of a miniaturised bulge tester for use at elevated temperatures*, [In] *2021 22nd International Conference on Thermal, Mechanical and Multi-Physics Simulation and Experiments in Microelectronics and Microsystems (EuroSimE)*, St. Julian, Malta, 2021: 1-6. <https://doi.org/10.1109/EuroSimE52062.2021.9410834>
- [22] ZHANG X.H., LIU B.Q., ZHOU F., *Pixel gray value correction for wide angle view image*, *Proceedings of the SPIE*, Vol. 9811, MIPPR 2015: Multispectral Image Acquisition, Processing, and Analysis, 2015: 981113. <https://doi.org/10.1117/12.2204731>
- [23] TANG X., WANG Q., X. MA X.J., GAO Z.D., MENG J., *Determination of the inner-surface profile of a capsule using chromatic confocal spectroscopy*, *Chinese Optics* **13**(2), 2020: 266-272.
- [24] ZAKRZEWSKI A., JUREWICZ P., KORUBA P., CWIKLA M., REINER J., *Characterization of a chromatic confocal displacement sensor integrated with an optical laser head*, *Applied Optics* **60**(11), 2021: 3232-3241. <https://doi.org/10.1364/AO.421382>
- [25] YU Q., ZHANG Y., ZHANG Y., CHENG F., SHANG W., WANG Y., *A novel chromatic confocal one-shot 3D measurement system based on DMD*, *Measurement* **186**, 2021: 110140. <https://doi.org/10.1016/j.measurement.2021.110140>
- [26] BAI W., LIANG D., CHEN W., CHYU M.K., *Investigation of ribs disturbed entrance effect of heat transfer and pressure drop in pin-fin array*, *Applied Thermal Engineering* **162**, 2019: 114214. <https://doi.org/10.1016/j.applthermaleng.2019.114214>
- [27] LI W.T., HUANG B.H., BI Z.B., *Analysis and Application of Thermal Stress Theory*, China Electric Power Publishing House, 2004: 89-90.
- [28] ABDOLLAHI A., NORRIS S.E., SHARMA R.N., *Heat transfer measurement techniques in microchannels for single and two-phase Taylor flow*, *Applied Thermal Engineering* **162**, 2019: 114280. <https://doi.org/10.1016/j.applthermaleng.2019.114280>

*Received December 28, 2023
in revised form February 26, 2024*